Journal of Power Sources 594 (2024) 234001

Contents lists available at ScienceDirect

Journal of Power Sources

journal homepage: www.elsevier.com/locate/jpowsour

Elucidating the role of $La_2NiO_{4\pm\delta}$ (LNO) nanoparticles in modulating chromium poisoning in LSM air electrodes of solid oxide cells: A study on oxygen reduction and evolution reactions

Hirad Salari [a], Arsalan Zare [a], Alireza Babaei [a,*], Hamid Abdoli [b,**], Hamed Aslannejad [c]

[a] School of Metallurgy and Materials Engineering, College of Engineering, University of Tehran, Tehran, Iran
[b] Renewable Energy Research Department, Niroo Research Institute (NRI), Tehran, Iran
[c] Copernicus Institute of Sustainable Development, Utrecht University, 3584 CS, Utrecht, the Netherlands

HIGHLIGHTS

- LNO impregnation improved LSM's ORR and OER performance.
- $LaCrO_3$ formation was detected after LNO/Cr reaction.
- LSM.LNO anode showed a stable behavior against Cr-poisoning.
- Gradual formation of $LaCrO_3$ continuously impeded the ORR activity of the LSM.LNO cathode.
- Detrimental phase formation was totally inhibited in the LSM.LNO anode.

GRAPHICAL ABSTRACT

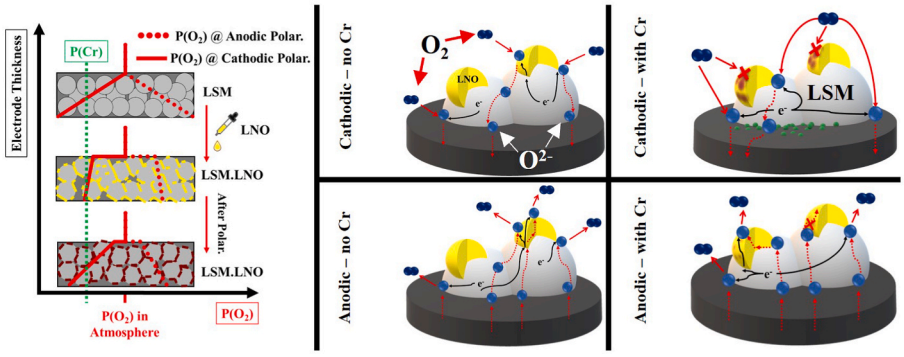

ARTICLE INFO

Keywords:
Solid oxide cell
Cr poisoning
LNO-Infiltrated LSM
Air electrode
Electrochemical evaluation
DRT

ABSTRACT

As the solid oxide cells (SOCs) are becoming durable, their air electrode materials require investigation for their tolerance against chromium (Cr) poisoning. Herein, $La_2NiO_{4\pm\delta}$ (LNO), a highly electroactive and nucleation agent-free material, is infiltrated into the $(La,Sr)MnO_{3-\delta}$ (LSM) backbone to diagnose its' influence on the Cr-poisoning of LSM. While the non-impregnated LSM's degrades by Cr contaminant, LNO-infiltrated LSM (LSM.LNO) shows less sensitivity to Cr presence specifically during the electrolysis mode. LNO's presence inhibits the formation of detrimental phases at the electrode/electrolyte interface during the anodic polarization in Cr-containing ambient. Moreover, surface promotion by LNO nanoparticles reduces, but not inhibits, the formation of undesirable phases during the cathodic polarization in the Cr presence. According to the electrodes' overpotential trends, the electrochemical impedance spectroscopy (EIS) responses in addition to the distribution of the relaxation times (DRT) analysis, the presence of Cr alters the LSM.LNO's electrochemical characteristics via reacting with the nanoparticles. As the XRD analysis proves, $LaCrO_3$ formation on the LNO nanoparticles' surface gradually decays the LSM.LNO's cathodic performance. However, LNO's higher activity for oxygen

* Corresponding author.
** Corresponding author.
E-mail addresses: alireza.babaei@ut.ac.ir (A. Babaei), hamidabdoli@yahoo.com (H. Abdoli).

https://doi.org/10.1016/j.jpowsour.2023.234001
Received 8 October 2023; Received in revised form 14 November 2023; Accepted 21 December 2023
Available online 9 January 2024

evolution than oxygen reduction reaction accompanied by slower LNO/Cr reaction kinetics during anodic polarization improve and stabilize the LSM.LNO's anodic performance in Cr-containing environment.

1. Introduction

One of the significant aspects guaranteeing the endurance of solid oxide cells' (SOCs) air electrode is the materials' resistivity towards the presence of chromium (Cr) species. In the SOC operational condition, a Cr_2O_3 scale forms on the surface of metallic interconnects, leading to the vaporization of CrO_3 and $CrO_2(OH)_2$ in the gas phase [1–4]. In this regard, developing Cr-tolerant electrode materials and coated interconnects with suppressed Cr volatilization were the object of many studies during recent years [1,2,5–9]. Two primary mechanisms have been attributed to Cr poisoning, including: 1) chemical reaction of Cr content with nucleation agents (e.g., Mn, Sr) in both solid oxide fuel and electrolysis cell (SOFC and SOEC) modes; and 2) direct electrochemical reduction of Cr containing phases on the active sites in SOFC mode [1]. Regardless of which poisoning mechanism is dominating, determining how the electrodes' oxygen reduction and evolution reactions (ORR and OER) kinetics would vary in the presence of Cr strongly depends on the electrodes' composition and physiochemical characteristics [10–12].

Perovskite (La,Sr)MnO_3 (LSM) material has been extensively studied as a promising air electrode for SOCs. However, some drawbacks limited LSM's exploitation, including its' poisoning by Cr content and its' negligible ionic conductivity [13]. The major detrimental products formed by the reaction of Cr with the LSM electrode are Cr_2O_3, (Cr, Mn)$_3O_4$, and $SrCrO_4$ solid phases producing at variable conditions [10,12,14–17]. Under SOFC mode, the Mn oxidation state becomes reduced, leading to the LSM's electrochemical activation because of the simultaneous formation of Mn^{2+} ions and oxygen vacancies on the LSM's surface [18,19]. In the presence of Cr, the Mn^{2+} ions, which were readily migrated towards the electrolyte surface, result in the formation of Cr_2O_3 and (Cr,Mn)$_3O_4$ detrimental phases [12,15–17]. Formation of these phases will not only occupy the triple phase boundaries (TPBs), but also deteriorate the oxygen ion transfer (charge transfer subprocess) from the LSM electrode to the electrolyte [1,3,12–17]. Under SOEC mode, LSM will experience an initial deactivation stage because of the simultaneous Sr segregation and oxygen vacancies annihilation after anodic current passage. Subsequently, an improvement will occur because of the TPB extension after crack formation near the electrode/electrolyte interface. Moreover, as the final stage is usually accompanied by the delamination of the LSM anode, it was suggested that the entrapment of the accumulated oxygen gas within the electrode/electrolyte interface resulted in the formation of LSM nanoparticles in this region leading to the electrode's failure [10,20,21]. Furthermore, it was revealed that after exposure to the Cr-species the transformation associated with the LSM anode would become accelerated as solid $SrCrO_4$ and Cr_2O_3 phases formed near the interfacial region [10].

A practical approach for the simultaneous enhancement of electrode performance and Cr tolerance is the surface decoration of the air electrodes using electrochemically active nanoparticles such as Pd, PdO_x [22], Gd-doped CeO_2 (GDC) [23,24], Y_2O_3-stabilized Bi_2O_3 (YSB) [25], $Ba_{0.5}Sr_{0.5}Co_{0.8}Fe_{0.2}O_{3-\delta}$ (BSCF) [26], Ag, $La_{0.8}Sr_{0.2}FeO_3$ (LSF), CeO_2 [27], $La_2Ni_{0.5}Co_{0.5}O_4$ (LNC) [28], and $La_2NiO_{4\pm\delta}$ (LNO) [29]. This approach culminates in TPB extension to the electrode's bulk and less dependency of the LSM electrode on the electrode/electrolyte interface for ORR and OER [30]. Chen et al. [24] reported that infiltration of GDC into the LSM backbone triggered the reduction of the electrode's cathodic and anodic overpotentials ($\eta_{cathodic}$ and η_{anodic}, respectively) from 0.33 to 0.025 V in SOFC mode and 0.32 to 0.03 V in SOEC mode at 800 °C under 200 mA cm^{-2} current density. It was mentioned that GDC incorporation prevented the electrode's delamination during the anodic current passage [24]. As an effective mitigation strategy against Cr poisoning of LSM-based electrodes, Wang et al. [23] proposed that GDC impregnation promoted the cathode's Cr tolerance in which $\eta_{cathodic}$ increased by only 15 mV after 1 h of cathodic polarization under 200 mA cm^{-2} at 900 °C, while in the case of the bare LSM electrode, it was increased by 270 mV under the same testing conditions. Recently, Huang et al. [31] incorporated a hybrid catalyst, including $BaCe_{0.8}Gd_{0.2}O_{3-\delta}$ and $BaCO_3$, into the LSM cathode. This coating led to a stable $\eta_{cathodic}$ in the range of 580 to 490 mV after 10 h polarization under 200 mA cm^{-2} at 800 °C in the presence of Cr [31]. It was indicated that the reaction between this coating and Cr resulted in the formation of less destructive phases including $BaCrO_4$ and GDC nanoparticles.

LNO Ruddlesden-Popper (R-P) phase has been proposed as one of the most promising materials that could improve electrode's performance and stability via impregnation into conventional cathodes [32–36]. Akbari et al. [29] revealed that the presence of LNO nanoparticles into the LSM backbone reduced the polarization resistance (R_P) of LSM around 90 % at 800 °C by enhancing the electrode's surface exchange kinetics. However, R_P of the LNO-infiltrated LSM electrode increases during anodic and cathodic current passage which was much more severe in the latter one. In another study, introduction of LNO coating via impregnation into the $PrBa_{0.5}Sr_{0.5}Co_{1.5}Fe_{0.5}O_{5+\delta}$ (PBSCF) was reported to improve the Cr poisoning tolerance of the electrode [32]. During cathodic polarization, while bare PBSCF electrode's $\eta_{cathodic}$ increased parabolically due to the gradual reaction of Cr and the segregated BaO on the electrode's surface, the LNO-coated electrode showed an improved stable performance [32]. In the other studies regarding LNO's Cr-poisoning, Lee et al. [37] and Schrödl et al. [38] reported the formation of $LaCrO_3$, $LaNiO_3$, and $LaCr_{1-x}Ni_xO_3$ phases on the surface of LNO which were resulted in diminution of the LNO electrode's electrochemical performance. Solodyankin et al. [39] investigated the degradation mechanism of LNO-based electrodes in contact with Cr-containing interconnects. Based on the formation of $LaCrO_3$ on the surface of the LNO functional layer during cathodic polarization, they suggested that the electrochemical reduction of Cr species on the cathode's surface caused $LaCrO_3$ formation [39,40]. This conclusion was drawn since, under anodic polarization, Cr trace was found on the current collector instead of the LNO functional layer [39]. These observations demonstrate that LNO's promising features including high electrochemical activity and low susceptivity to react with Cr, could be faded as a result of its' instability and phase changes during the operational condition of SOCs [35,37–39,41–45]. Hence, assessing the applicability of LNO infiltration into the LSM electrode requires further structural and electrochemical investigations under different operating conditions in the presence and absence of Cr.

This study investigates the electrochemical properties of the LSM and the role of surface decorating LNO nanoparticles in the presence of Cr using a three-electrode configuration. LNO-infiltrated and bare LSM electrodes were polarized anodically and cathodically by ±200 mA cm^{-2} at 800 °C in the absence and presence of Cr. Furthermore, electrochemical impedance spectroscopy (EIS) and distribution of relaxation times (DRT) analysis were exploited to evaluate the electrode's R_P along with its' electrochemical behavior towards ORR and OER during the current treatments. Even though the polarization curves and EIS measurements showed that the LNO-infiltrated cells would behave differently in the presence of Cr, these samples are more tolerant towards the Cr presence in the gas phase compared to bare LSM. Also, the electrodes' structural and chemical variation caused by Cr content were investigated after current passage.

2. Materials and methods

2.1. Cell fabrication

8 mol% Y_2O_3 stabilized ZrO_2 (YSZ, Tosoh, Japan) was mixed with 2 wt% polyvinyl butyral (Kuraray) to fabricate YSZ electrolyte pellets. The mixture was then dry pressed and sintered according to the procedure explained in our previous work [46]. Working, counter and reference electrodes (WE, CE, and RE) were applied on the YSZ electrolyte according to the three-electrode configuration. To prepare the working electrode, $(La_{0.80}Sr_{0.20})_{0.95}MnO_{3-X}$ (LSM, Fuel cell Materials) was ball-milled with Ink Vehicle (Fuel Cell Materials) and screen-printed to the electrolyte followed by air sintering at 1100 °C for 2 h. For the counter and reference electrodes, platinum paste (6082 Metalor) was applied on the opposite side of the YSZ electrolyte [29]. These electrodes were then air sintered at 850 °C for 20 min. WE and CE surface area were 0.5 cm^2.

0.5 M $La_2NiO_{4\pm\delta}$ (LNO) precursor solution was prepared by dissolving $La(NO_3)_3.6H_2O$ (99 %, Merck), $Ni(NO_3)_2.6H_2O$ (99 %, JDH) and citric acid (CA) (99 %, Samchun) with 2:1:3 M ratio in deionized water. At each step of infiltration, a droplet of the solution was wet-infiltrated into the LSM backbone followed by firing at 350 °C for 1 h and calcining at 900 °C for 1 h. The whole impregnation sequence was repeated 5 times to achieve the lowest R_P value [29].

2.2. Electrochemical testing

Fabricated cells were electrochemically analyzed in the absence and presence of Cr source. Fig. S1 of the supporting information file represents the schematic picture of the testing setup when the Cr source is present. A platinum mesh was exploited as the current collector on top of LSM and LNO-infiltrated LSM (LSM.LNO) working electrodes. 1 cm^2 of a 430 stainless steel was placed on top of the platinum mesh as the chromium source for the investigation of the poisoned LSM (P.LSM) and LSM.LNO (P.LSM.LNO) electrodes. Electrochemical behavior of the electrodes was studied by means of Chronopotentiometry (CP) with a Metrohm Autolab potentiostat (PGSTAT302 N, Autolab) under ± 200 mA cm^{-2} cathodic and anodic currents at 800 °C. According to Eq. (1), $\eta_{cathodic}$ and η_{Anodic} were calculated from the cathodic and anodic potentials ($E_{cathodic}$, E_{anodic}) and the ohmic resistances (R_Ω) were derived from CP and electrochemical impedance spectroscopy (EIS) tests, respectively [16]. i in Eq. (1) represents the current density. By exploiting a current interruption technique, the iR contribution was deducted from the overpotential curves during the current treatment. EIS was performed in the frequency range of 100 kHz to 0.1 Hz with the AC amplitude of 10 mV.

$$E = \eta + iR_\Omega \quad \text{(Eq. 1)}$$

At the end of the current passage, the EIS spectra of the electrodes were also collected by applying a bias voltage of ±0.3 V. For more precise interpretation of the EIS responses, distribution of relaxation times (DRT) technique was conducted using DRT-tools open-source code, and the Tikhonov regularization was chosen for this analysis. The resistance associated to high, medium, and low frequencies of the EIS spectra was obtained from the integration of the surface area of the $\gamma(\tau)$ vs. Ln (τ) plot [47,48].

2.3. Characterization

To study the potential reactivity between LNO and Cr_2O_3, LNO powder (synthesized by sol-gel combustion method) was mixed with Cr_2O_3 (99.99 %, Merck Millipore) using an agate mortar and pestle, followed by heat treatment at 800 °C for 12 h. To investigate the formation of the LNO phase as well as LNO reactivity with the Cr_2O_3, X-ray diffraction (XRD) by a Philips 1730-PW X-ray diffractometer equipped with CuKα source was exploited. The chemical compatibility of LSM/LNO and LNO/YSZ mixtures (in 1:1 wt% ratio) were tested by means of XRD after heat treating the mixtures at 900 °C for 1 h followed by 12 h holding at 800 °C in air atmosphere. This calcination route was chosen to study the feasibility of occurrence of chemical reactions between the impregnated LNO nanoparticles and the LSM and YSZ compounds during the cell fabrication step as well as the electrochemical test procedure.

Microstructural characterization and elemental analysis of the electrodes' cross-sections were carried out by means of a field emission scanning electron microscope (FESEM, Tescan) in addition to an energy dispersive spectroscopy (EDS) detector.

3. Result and discussion

Fig. 1 illustrates the XRD patterns of the LSM/LNO (Fig. 1-a) and LNO/YSZ (Fig. 1-b) mixtures before and after heat treatment for 60 min at 900 °C followed by holding for 720 min at 800 °C. According to the XRD patterns, after heat treatment, no secondary phase formation is observable showing the chemical compatibility of the LSM/LNO and LNO/YSZ components in the studied temperature range. It was reported that the LNO and YSZ compounds are prone to react with each other at high sintering temperatures which is not applicable to the condition of this study [42,49]. Similar to the results in Fig. 1-a, the chemical compatibility between LNO and LSM was also previously investigated in which no variation was reported [29].

Fig. 2 depicts the polarization curves of the P.LSM and P.LSM.LNO (Fig. 2-a) in addition to their non-poisoned counterparts (Fig. 2-b) at 800 °C for 600 min under cathodic and anodic polarization. In Fig. 2-a, P.LSM sample's η_{anodic} slightly increases from 443 to 465 mV after 600 min. This behavior differs from that of the pure LSM (Fig. 2-b) in which η_{anodic} gradually reduces from 357 to 298 mV. It is evident that OER is prone to become enhanced during the anodic polarization in the absence of Cr. LSM's minor OER facilitation during the test could be attributed to the competition between the Sr segregation and crack formation at the LSM/YSZ interface resulting in increment of active areas for oxygen evolution [10,20,21]. Meanwhile, the presence of Cr species in the ambient slightly impeded LSM's OER kinetics resulting in small increase of η_{anodic} as similarly reported by Chen et al. [10]. It could be assumed that no Cr species electrochemically reduced at the LSM/YSZ interfacial region because of the oxidative condition under the anodic polarization. However, the presence of Cr in the gas phase could have easily disturbed the desorption of the oxygen species leading to the minor OER performance decay [10,17]. By further exploring the polarization curves in Fig. 2, it is evident that the incorporation of LNO nanoparticles into the LSM scaffold not only lowers η_{anodic} in both poisoned and non-poisoned electrodes due to the extension of the TPB area, but also alters the electrode's polarization trend [29,36]. As presented in Fig. 2-a, η_{anodic} of P.LSM.LNO electrode increases from 78 to 161 mV after about 120 min of polarization and become stable for the rest of the test. However, in Fig. 2-b, LSM.LNO's η_{anodic} raises gradually from 45 to 145 mV after 600 min. The gradual η_{anodic} increment in LSM.LNO anode represents that during the current passage LNO's electrochemical properties degraded because of LNO's surface reconstruction or other possible structural variations [33,35,41–43,50]. Nonetheless, as in P.LSM.LNO, such changes in LNO were concurrent with its' interaction with Cr, the initial OER decay and subsequent performance stabilization happened. Furthermore, it is evident that during the polarization tests the presence of LNO nanoparticles facilitated the OER, regardless of LNO's intrinsic changes or variation obligated by the presence of Cr species. The role of LNO impregnated nanoparticles in the poisoning ambient, is also observable in Fig. 2-a from comparing the P.LSM.LNO's E_{anodic} variations with P.LSMs during the current passage. At each current interruption, P.LSM electrode's E_{anodic} is approximately restored to the initial potential (prior to current passage), while in P.LSM.LNO sample the E_{anodic} restoration is not reproducible. In P.LSM.LNO during the initial 60–120 min, at each current interruption the starting points of E_{anodic}

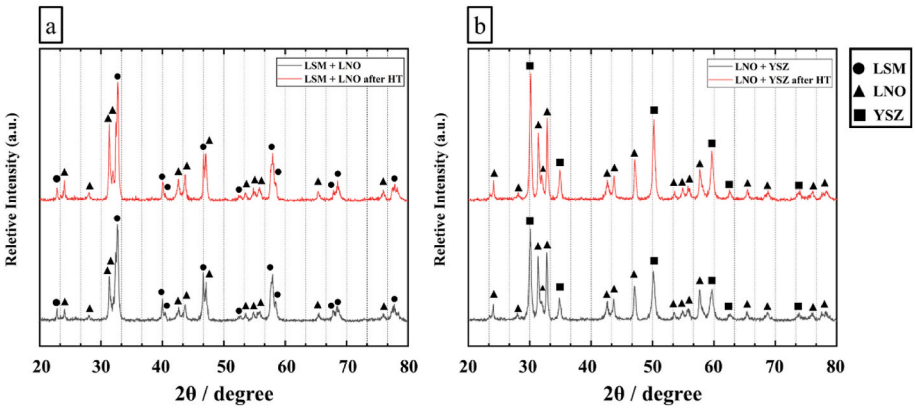

Fig. 1. XRD patterns of (a) LSM/LNO, and (b) LNO/YSZ mixtures (1:1 wt%) before and after heat treatment for 1 h at 900 °C followed by 12 h at 800 °C.

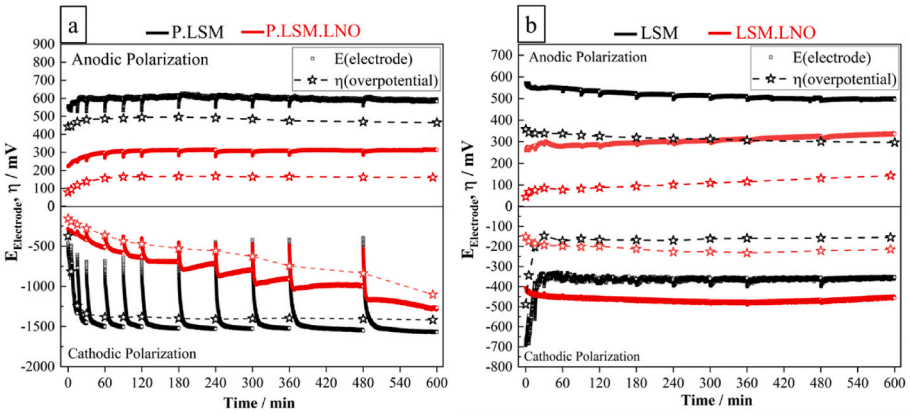

Fig. 2. Polarization curves for LSM and LSM.LNO in the presence (a) and in the absence (b) of chromium species, under anodic and cathodic current density of ±200 mA cm^{-2} at 800 °C.

slightly increases, however, after this period the E_{anodic} trend become stabilized. The different E_{anodic} trend of P.LSM.LNO indicates that the electrode's electrochemical nature altered due to the possible chemical interactions between LNO and Cr species [10,16,17,51].

During cathodic polarization (Fig. 2-a), P.LSM's $\eta_{cathodic}$ rapidly surges from 373 mV to about 1400 mV within 60 min followed by a slight increase to 1419 mV after 600 min. This behavior represents that the presence of Cr in the gas phase had a strong inhibiting effect on the electrode's ORR [12]. Contrarily, same as the previous studies on LSM's ORR behavior in Cr-free atmosphere, the LSM sample became activated and its' performance significantly enhanced which is conspicuous by the $\eta_{cathodic}$ reduction from 500 mV to 155 mV (Fig. 2-b) [18,19]. However, in the infiltrated samples, abrupt changes are neither observable in the case of P.LSM.LNO nor LSM.LNO. In the former, $\eta_{cathodic}$ gradually reaches 1100 mV from 157 mV within 600 min (Fig. 2-a), while in the latter $\eta_{cathodic}$ is slightly increased between 151 and 215 mV within 600 min of cathodic polarization (Fig. 2-b). These low overpotential values with such stability were also reported in previous studies on surface decorated LSM electrodes including GDC– [11,23], LNO– [29] and $Ba_{0.5}Sr_{0.5}Co_{0.8}Fe_{0.2}O_{3-\delta}$ (BSCF)– [26] impregnated LSM electrodes. It was previously described that the incorporation of nanoparticles by either ion conducting or MIEC phases could attenuate the LSM's activation behavior under the cathodic polarization in Cr-free atmosphere [11]. Moreover, the continuous overpotential increase similar to the one happened in P.LSM.LNO cathode was also reported on (La,Sr)(Co,Fe)$O_{3-\delta}$ (LSCF) and PBSCF electrodes [32,51,52]. Gradual formation of Cr-containing solid insulator phases on the LSCF and PBSCF surface and occupation of the electrochemically active sites were asserted to be responsible for the overpotential continuous increment. At the initial stages P.LSM.LNO cathode behaved like LSM.LNO where $\eta_{cathodic}$ and $E_{cathodic}$ of P.LSM.LNO were lower and much more stable than P.LSM samples. Nonetheless, by further current passage $\eta_{cathodic}$ and $E_{cathodic}$ began to continuously increase similar to the LSCF and PBSCF in previous studies. Therefore, it would be possible to assign the $\eta_{cathodic}$ trend in P.LSM.LNO to the gradual reaction of Cr content with the LNO nanoparticles. These results indicate that the co-existence of Cr and LNO is accompanied by dynamic changes in the electrochemical properties of the electrodes towards ORR and OER.

Fig. 3 illustrates the effects of current passage on the R_P variation in LSM, P.LSM, LSM.LNO, and P.LSM.LNO samples during the anodic and cathodic polarizations. Contrary to the rather stable OER behaviors of LSM and P.LSM electrodes (Fig. 2-a and -b), the P.LSM's R_P starts with an initial abrupt decrease (<5 min) and continues in a reverse direction for the remaining time. In Fig. 3-a, R_P of P.LSM reduces from 3.44 to 2.66 Ω cm^2 and then increases to 3.59 Ω cm^2 after 600 min. According to Fig. 3-b, anodic polarization of LSM is, however, accompanied by the electrode's deactivation and R_P increment from 7.55 to 13.51 Ω cm^2, only after 15 min which was then continued by an improvement in R_P reaching 6.47 Ω cm^2 after 600 min. While the initial increment and following reduction in R_P for LSM electrodes are known and well demonstrated before [10,21], the different trend of R_P in the P.LSM (Fig. 3-a) electrode could be ascribed to the presence of Cr species. A possible explanation for this R_P trend in P.LSM is that the Cr species shorten the duration of each distinct stage during the anodic polarization and our resistance measurement was not able to detect the initial rapid deactivation stage (<5 min) [10,21]. For the infiltrated electrodes in Fig. 3-a and -b, R_P variations are consistent with the E_{anodic} and η_{anodic} tendencies (Fig. 2-a and -b). In P.LSM.LNO (Fig. 3-a), within 120 min of

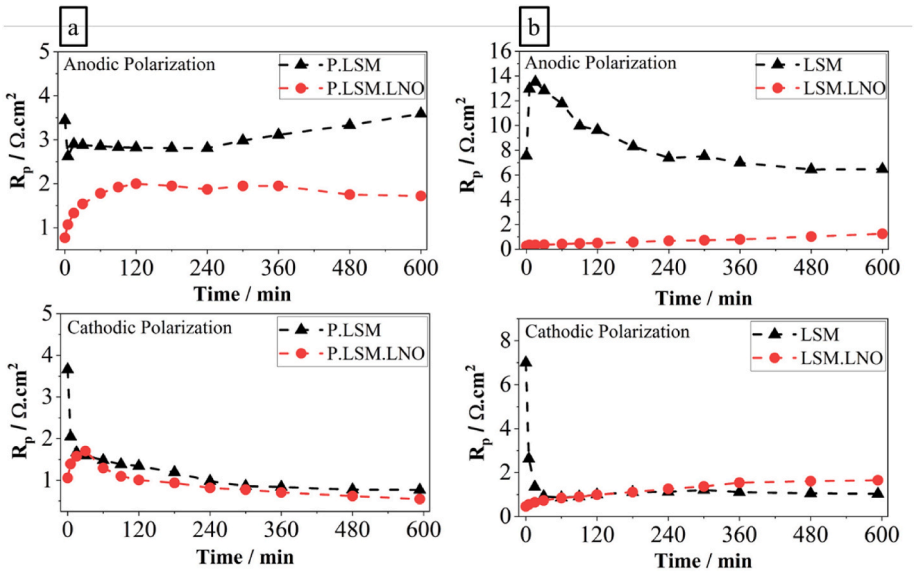

Fig. 3. Polarization resistances of LSM and LSM.LNO in the presence (a), and in the absence (b) of chromium during the cathodic and anodic current treatment obtained by EIS measurement after interrupting the current at OCP and 800 °C.

anodic polarization, R_P increases from 0.77 to 2.01 Ω cm^2 and then mildly reduces to 1.72 Ω cm^2 after 600 min, which is less than half of the non-infiltrated P.LSM anode. In LSM.LNO (Fig. 3-b), R_P continuously increases from 0.26 to 1.24 Ω cm^2 after 600 min. The R_P trends of the infiltrated samples demonstrate that the possible structural transformation in the LNO nanoparticles caused the continuous R_P increment in LSM.LNO sample. Meanwhile, the simultaneous effects of changes associated with LNO and Cr-poisoning led to the initial deterioration of the electrochemical properties and subsequent R_P stabilization in P.LSM.LNO.

In Fig. 3-a, under cathodic current, R_P of the P.LSM sample drastically drops from 3.66 to 1.66 Ω cm^2 within 15 min, and then moderately reduces to 0.77 Ω cm^2 after 600 min. A similar behavior is visible in LSM electrode (Fig. 3-b) where R_P rapidly decreases from 7 to 1.35 Ω cm^2 after 15 min followed by ending up at 1.03 Ω cm^2 after 600 min. Considering the trends associated with P.LSM's $\eta_{cathodic}$ and R_P, it could be concluded that the presence of Cr in gas phase severely interrupted ORR subprocesses, but the formation of oxygen vacancies has not been inhibited, as the electrode's R_P reduced after cathodic polarization [12, 16]. Furthermore, in Fig. 3-a, R_P of the P.LSM.LNO cathode increases from 1.05 to 1.70 Ω cm^2 after 30 min followed by a gradual reduction to 0.55 Ω cm^2 after 600 min. In Fig. 3-b, R_P of the LSM.LNO cathode, like LSM.LNO anode, increases from 0.46 to 1.65 Ω cm^2 after 600 min possibly because of the changes occurred within the LNO structure. Beside the R_P increment within the initial 30 min of cathodic polarization, the trends associated with P.LSM.LNO's R_P, $\eta_{cathodic}$, and $E_{cathodic}$

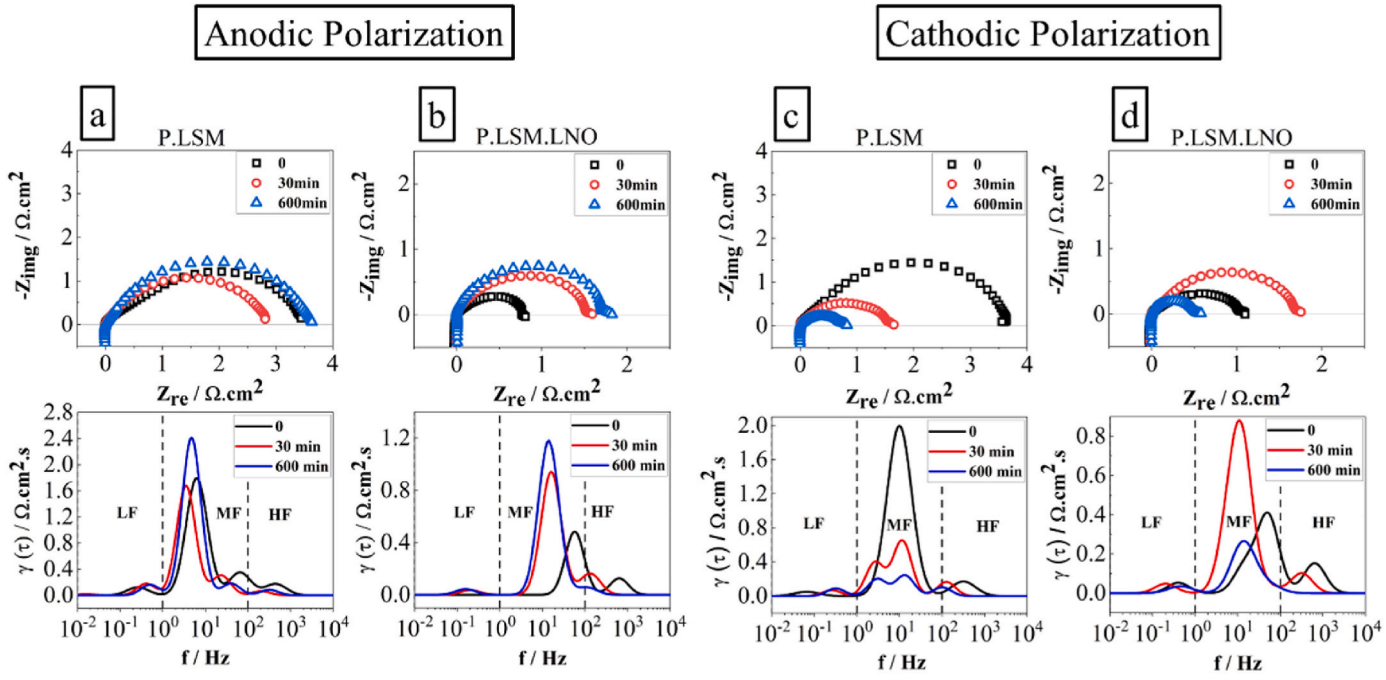

Fig. 4. EIS spectra and its' corresponding DRT for (a) LSM, (b) LSM.LNO under anodic polarization, (c) LSM and (d) LSM.LNO under cathodic polarization in the presence of Cr at 800 °C.

vary similar to the ones in P.LSM cathode. Considering the gradual $\eta_{cathodic}$ increment and the R_P trend in P.LSM.LNO cathode, it would be possible to find the reasons behind these variations by some assumptions. In this regard, it is plausible that during the initial 30 min LNO nanoparticles partially lost their electrochemical activity and by further exposure to the Cr-containing atmosphere occurrence of a secondary phase formation led to the activation of the LSM backbone and obtaining the observed R_P and $\eta_{cathodic}$ trends. As these variations were not seen in neither LSM.LNO nor P.LSM, it would be reasonable to consider that the R_P and $\eta_{cathodic}$ variations in P.LSM.LNO sample are because of the LNO/Cr interactions.

Fig. 4 depicts the EIS and DRT responses of the P.LSM and P.LSM.LNO electrodes at OCP condition after anodic and cathodic polarizations for 0, 30 and 600 min. DRT analysis helps to deconvolute the electrode's responses while demonstrating the contribution of OER/ORR subprocesses to the total polarization resistance [46,47,53]. Additionally, the results regarding the electrochemical responses of LSM and LSM/LNO in the absence of Cr are also provided in Fig. S2 of the supporting information. The contribution of High, medium, and low frequency (HF, MF, LF) resistances to the total polarization resistance listed in Table 1, was calculated from the integration of the $\gamma(\tau)$ vs. Ln (τ) plot's surface area [48,54–56]. For better elucidation, the ranges (10^{-2}–1), (1–100) and (100–10^4) Hz are designated as LF, MF and HF, respectively [48,54,57,58]. According to Fig. 4, the MF peaks are altered more substantially showing that the subprocesses assigned to this frequency range were mainly responsible for the total R_P changes in all the samples. The subprocesses regarding this frequency range are normally attributed to the oxygen dissociative adsorption/associative desorption as well as the surface diffusion of the oxygen ions [29,54]. According to Fig. 4-a, R_P of the P.LSM anode changes due to a reduction in MF resistance from 3.13 to 2.54 Ω cm^2 after 30 min, which is followed by an increase to 3.30 Ω cm^2 after prolonging for 600 min. The HF and LF peaks which are remained rather unchanged are attributed to the charge transfer (oxygen ions transfer from electrode to the electrolyte) and oxygen gas diffusion, respectively [16,54,57,58]. According to Fig. 3-a and 4-a, R_P of P.LSM could have varied as a consequence of the competition between the constructive effect of LSM nanoparticles formation and the destructive reaction of Cr with the segregated Sr near the TPB area [4,10,20,21]. In P.LSM.LNO anode (Fig. 4-b), MF resistance increases from 0.53 to 1.35 and 1.67 Ω cm^2 after 30 and 600 min, respectively. Thus, the initial performance decay of the P.LSM.LNO anode was due to the partial deactivation of the LNO nanoparticles surface and the electrode's deteriorated surface exchange kinetics. As shown in Fig. 4-c, the P.LSM cathode's R_P varies due to the formation of oxygen vacancies on the LSM's surface resulting in MF resistance reduction [11,12,16]. The EIS and DRT analysis responses of the P.LSM.LNO cathode in Fig. 4-d depicts that the initial increase and the subsequent reduction of R_P is also affected by variation of the surface exchange reaction kinetics leading to the electrode's MF resistance alteration. As listed in Table 1, the MF resistance of the P.LSM.LNO cathode increases from 0.72 to 1.52 Ω cm^2 after 30 min followed by reduction of MF resistance to 0.49 Ω cm^2 after 600 min.

The initial increase of R_P in both anodic and cathodic polarizing conditions is notable and implies that the infiltrated samples would have initially experienced an electrochemical activity decay regardless of the polarization condition, but their further behavior depend on the anodic or cathodic nature of the polarization as well as the Cr/LNO interaction. According to the previous investigations on the R-P phase surface reconstruction specifically the LNO material, segregation of the La content towards the LNO's surface and subsequent formation of La_2O_3 on the nanoparticles' surface was noticed [43,44,50,59]. This structural variation could be a plausible explanation for either the infiltrated electrodes' continuous performance decay in the Cr-free ambient or the initial deterioration of the electrocatalytic activity in the presence of Cr [41–44,50]. According to the previous experimental analysis and thermodynamical calculations regarding LNO's phase transformation, it was well established that the formation of La_2O_3, $La_3Ni_2O_{7-\delta}$, and $La_4Ni_3O_{10-\delta}$ phases is thermodynamically favoured at 600–800 °C which is the operating range of the intermediate temperature SOCs (IT-SOCs) [43,44]. It was also presented that LNO's surface reconstruction would become extremely facilitated under conditions favourable for ORR, if this material has a direct contact with an electrocatalyst (e.g., Pt) which is in our case is LSM itself [50]. In addition, the reconstruction of the LNO's structure is not confined to the OCP condition as it was also previously noticed in LNO containing electrodes under both cathodic and anodic polarizations [41,42]. Furthermore, Sharma et al. [60] justified the Cr-poisoning of $La_{0.8}Sr_{0.2}CoO_3$ air electrode under anodic polarization on the ground of the reaction between the segregated La_2O_3 and Cr content in the gas phase. It was confirmed that the main products of this reaction were $LaCrO_3$ and La_2CrO_6 phases [60]. Hence, one reason behind the R_P reduction under cathodic condition as well as the stabilized behavior under anodic condition, could be the formation of $LaCrO_3$ because of the reaction between La_2O_3 and Cr. $LaCrO_3$ would not totally deteriorate the electrochemical performance of the electrodes since it possessed a reasonable electrocatalytic activity as well as an electronic conductivity of 0.33 S cm^{-1} in air at 800 °C [37,61,62].

Additionally, P.LSM.LNO's performance under cathodic and anodic polarizations clearly implicates a more detrimental effect of the Cr content on the P.LSM.LNO electrode's ORR rather than OER performance. Previously, Egger et al. [43] showed that the LNO electrode was more prone to Cr poisoning under SOFC than SOEC mode. The higher electrochemical stability of P.LSM.LNO under anodic condition might be due to the proposed OER mechanisms by Sdanghi et al. [63]. It was stated that in LNO air electrode, while oxygen transportation is only narrowed to the surface diffusion during ORR, it benefits from the additional path of interstitial sites (bulk) during OER. So, even if the LNO's surface becomes partially deactivated by either the less active or insulator phases, this material's bulk would maintain its' activity during OER.

Cross-sectional FESEM micrographs of the examined electrodes after 600 min of polarization in the presence of Cr are depicted in Fig. 5. Results of EDS analysis are also listed in Table 2 for the selected points.

Table 1
Resistance of the electrodes corresponding to Fig. 4 obtained from the P.LSM and P.LSM.LNO samples' DRT plots.

Polarization	Electrode	Time (minutes)	HF resistance (Ω.cm^2)	MF resistance (Ω.cm^2)	LF resistance (Ω.cm^2)	Total resistance (Ω.cm^2)
Anodic	LSM/Cr	0	0.37	2.89	0.18	3.44
		30	0.07	2.54	0.25	2.86
		600	0.11	3.30	0.19	3.60
	LSM.LNO/Cr	0	0.24	0.53	0.00	0.77
		30	0.16	1.35	0.05	1.56
		600	0.05	1.67	0.06	1.78
Cathodic	LSM/Cr	0	0.27	3.34	0.08	3.69
		30	0.14	1.36	0.10	1.60
		600	0.06	0. 62	0.10	0.78
	LSM.LNO/Cr	0	0.30	0.72	0.07	1.09
		30	0.15	1.52	0.07	1.74
		600	0.01	0.49	0.05	0.55

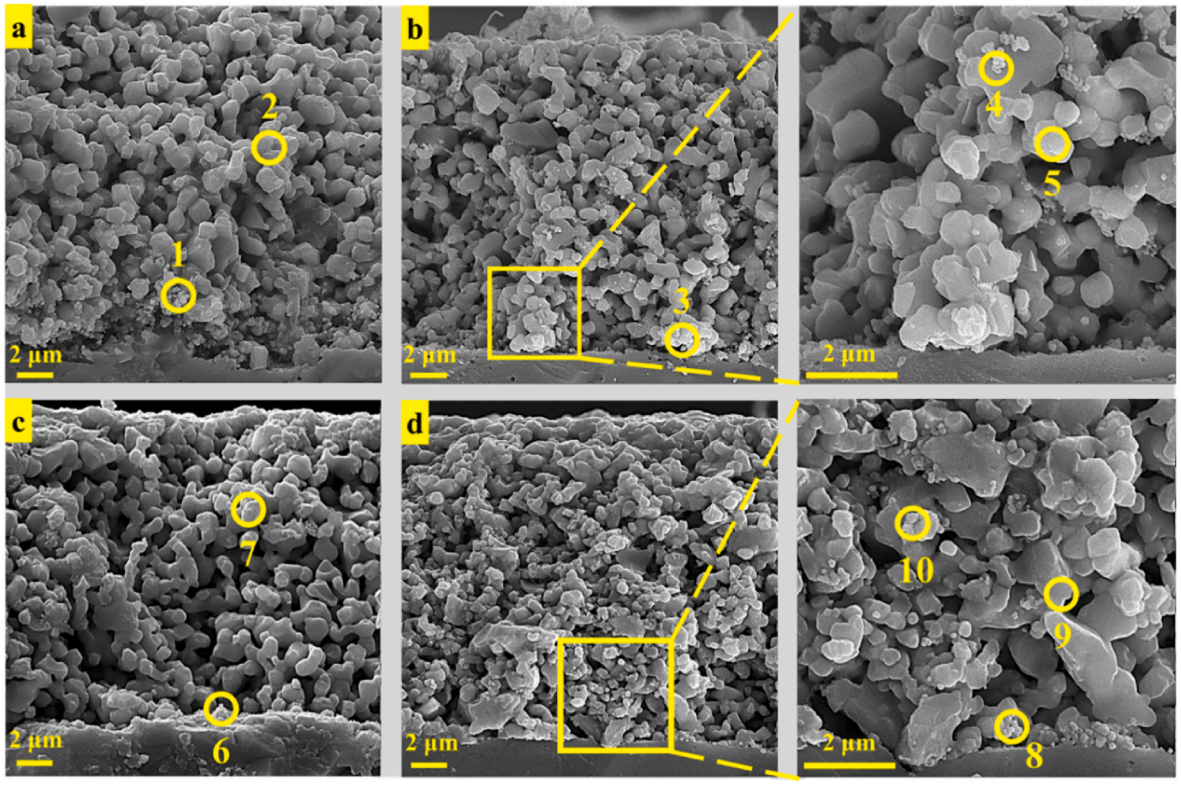

Fig. 5. FESEM images for the P.LSM and P.LSM.LNO samples after 10 h of anodic polarization (a and b, respectively), and cathodic polarization (c and d, respectively). (Circles represent the points which EDS analysis obtained from).

Table 2
EDS analysis of the points noted in Fig. 5.

Elements	Point 1 (wt %)	Point 2 (wt %)	Point 3 (wt %)	Point 4 (wt %)	Point 5 (wt %)	Point 6 (wt %)	Point 7 (wt %)	Point 8 (wt %)	Point 9 (wt %)	Point 10 (wt %)
O	28.23	29.48	27.33	27.61	29.61	25.95	29.12	27.70	29.45	27.19
Cr	4.60	0.00	2.45	1.40	0.00	6.38	0.00	3.18	0.00	2.03
Mn	17.35	20.95	17.61	17.94	19.95	15.48	21.31	12.61	22.50	19.48
Sr	18.34	16.45	17.49	16.96	16.64	6.18	16.22	13.98	16.43	15.12
Y	–	–	–	–	–	4.40	–	2.98	–	–
Zr	–	–	–	–	–	18.47	–	12.36	–	–
La	31.48	33.12	32.63	34.03	33.80	23.14	33.35	25.16	31.12	34.45
Ni	–	–	2.49	2.06	0.00	–	–	2.03	0.50	1.73
Total	100	100	100	100	100	100	100	100	100	100

As shown in Fig. 5-a, at the area near the electrolyte's surface, distinctive nanoparticles were formed as a consequence of P.LSM anodic polarization. The appearance of these particles could be attributed to the formation of Cr_2O_3, CrO_x and $SrCrO_4$ phases near the LSM/electrolyte interface which was well addressed in a prior study [10]. These observations were confirmed by considering different Sr and Cr contents in points 1 and 2. The EDS results of point 1 verifies the presence of 18.34 wt% (8.04 at.%) Sr accompanied by 4.60 wt% (3.40 at.%) Cr, suggesting the possible formation of Sr-Cr nucleus. In point 2, 16.45 wt% (7.08 at. %) Sr is present but no sign of Cr content is detectable which elucidates the fact that the reaction zone was mainly limited to the interfacial region. The moderate reduction of the surface exchange kinetics (MF resistance increment) of P.LSM anode which is shown in Fig. 4-a could also be attributed to the formation of such insulator phases close to the TPB area. Meanwhile, in P.LSM.LNO (Fig. 5-b), formation of the distinct nanoparticles near the interface is not observable after polarization. The EDS analysis from points 3 and 4 elucidates LNO nanoparticles existence, as some traces of Ni including 2.49 wt% (1.66 at.%) and 2.06 wt% (1.37 at.%) are detected in these points. Likewise, in points 3 and 4, 2.45 wt% (1.85 at.%) and 1.40 wt% (1.05 at.%) Cr content are also noticeable, respectively. Thus, the direct reaction of Cr content with the LNO nanoparticles seems plausible. Additionally, by examining the point 5 it is evident that the LNO-free areas do not contain Ni and Cr, so it would be possible that the LSM particles did not react with the Cr contaminants which is consistent with the previous studies [1]. Absence of the Sr-rich particles at the P.LSM.LNO anode/electrolyte interface suggests that although the LNO nanoparticles' surface were possibly altered by the Cr content, their presence still inhibited or deferred the segregation of the SrO species. Incorporation of LNO nanoparticles, extended the active sites for OER to the electrode's bulk, consequently less oxygen ions would have incorporated into the LSM lattice near the interfacial region. Thus, the segregation of Sr content which was reported to be due to the oxygen ions incorporation into the LSM structure did not occur in P.LSM.LNO as severe as it happened in P.LSM anode [10,21,64].

The P.LSM electrode's micrograph after cathodic polarization is illustrated in Fig. 5-c. Despite no significant change in the electrode's microstructure, formation of secondary phases on the electrolyte surface is visible, e.g., point 6. The corresponded EDS analysis shows the presence of 6.38 wt% (4.88 at.%) Cr at this region along with 15.48 wt%

(11.20 at.%) Mn, showing a likelihood of the reaction between Cr and Mn ions on the surface of the electrolyte. This reaction was explicitly noticed in former studies on the Cr poisoning of LSM cathode [7,12,15–17,65]. Meanwhile, finding no traces of Cr at regions far from the interface (e.g., point 7), implies that the poisoning reaction had been confined to the electrode/electrolyte interface. Fig. 5-d exhibits the P.LSM.LNO sample's cross-section after cathodic polarization. By comparing the EDS results for points 8,9, and 10, it is noticeable that 3.18 wt% (2.38 at.%) and 2.03 wt% (1.54 at.%) of Cr are spotted in points 8 and 10, respectively; however, no trace of Cr is detectable in point 9. This result could indicate that the presence of LNO nanoparticles resulted in entrapment of Cr content on this phase throughout the electrode's thickness. Moreover, since in LNO free points (e.g., points 7 and 9) no Cr content is found, it is reasonable to conclude that Cr did not react with LSM during the cathodic polarization same as the anodic polarization. Hence, it would be possible to assume that LNO directly reacted with Cr in gas phase through a nucleation agent that had been probably formed on the surface of LNO during the polarization (e.g., the segregated La). Furthermore, the lower amounts of Cr content at the interfacial region of P.LSM.LNO than P.LSM cathode demonstrates that lower volume of nucleation agents (e.g., Mn^{2+}) produced in the cathodically polarized P.LSM.LNO. However, in P.LSM cathode, Mn ions started reducing to Mn^{2+} just after the beginning of cathodic current passage. Furthermore, besides the interaction of Cr and LNO nanoparticles, it could be declared that the formation of Sr-Cr and Mn-Cr containing phases which are the main cause of LSM air electrode's Cr-poisoning were postponed or inhibited at the interfacial area of the P.LSM.LNO anode and cathode.

The EIS spectra presented in Fig. 4 were measured at OCP. However, a comprehensive evaluation of the electrode's R_P would have been obtained from the electrode's responses if the EIS spectra were also measured under a constant cathodic and anodic DC bias. Hence, in Fig. 6, EIS and DRT of the 600 min polarized P.LSM and P.LSM.LNO electrodes at ± 0.3 V DC bias are presented. Also, to precisely visualize the differences between the polarized samples before and after DC bias appliance, additional information is provided in Fig. S3 presenting the EIS spectra and DRT plots of the examined samples. Shown in Fig. 6-a, applying a high anodic potential of +0.3 V under OCP condition, severely reduces R_P for both P.LSM and P.LSM.LNO from 3.6 and 1.78 Ω cm^2 (Fig. 4-a and -b), to 0.21 and 0.11 Ω cm^2, respectively. It was previously explained that a high anodic potential simulates a condition in which the oxygen partial pressure (OPP) would increase and thereby R_P decrease [66,67]. Therefore, applying a +0.3 V DC voltage lowers the R_P in both electrodes, but the resistance value is still lower in case of the infiltrated electrode showing its' higher electrochemical activity. Based on the DRT analysis in Fig. 6-a and the DRT plot of the P.LSM and P.LSM.LNO electrodes in Fig. 4-a and -b, applying the anodic DC bias results in the reduction of LF and MF peaks' size in both P.LSM and P.LSM.LNO anodes. This variation shows that the higher OPP at the area near electrode/electrolyte interface is likely to facilitate the gas diffusion and oxygen surface exchange subprocesses. In the case of P.LSM.LNO sample, the MF and LF peaks are reduced in size and merged to form one small peak at the MF region. Such changes of the peaks in the DRT analysis of different air electrode materials were previously noticed in several studies [53,56,66–68].

As it is seen in Fig. 6-b, utilization of −0.3 V DC bias leads to a significant increase in R_P of P.LSM and P.LSM.LNO samples from 0.78 and 0.55 Ω cm^2 (Fig. 4-a and -b), to about 21.03 and 7.62 Ω cm^2, respectively. Comparing the DRT plots in Fig. 4-c and -d with Fig. 6-b, it is conspicuous that the cathodic DC bias in the presence of Cr deteriorates the P.LSM and P.LSM.LNO cathodes performance by limiting the subprocess associated with LF and MF. A cathodic DC bias provides an intense OPP gradient across the electrode's thickness in which the oxygen content is primarily consumed at the electrode/electrolyte area resulting in a poor supply of oxygen gas for dissociative adsorption in the active area [69]. As the Cr content was available during the introduction of −0.3 V DC bias to the P.LSM sample, Cr inhibiting effect on oxygen exchange in addition to the poor oxygen supply resulted in an increase of the resistances correspond to the surface exchange reaction and gas diffusion, respectively. Also, a semi-linear Warburg type impedance is observable in the HF section of the P.LSM electrode's response due to the formation of Cr containing phases at the interfacial region and their impeding effect on the charge transfer subprocess [12]. A more significant R_P increment is evident in cathodically polarized P.LSM rather than

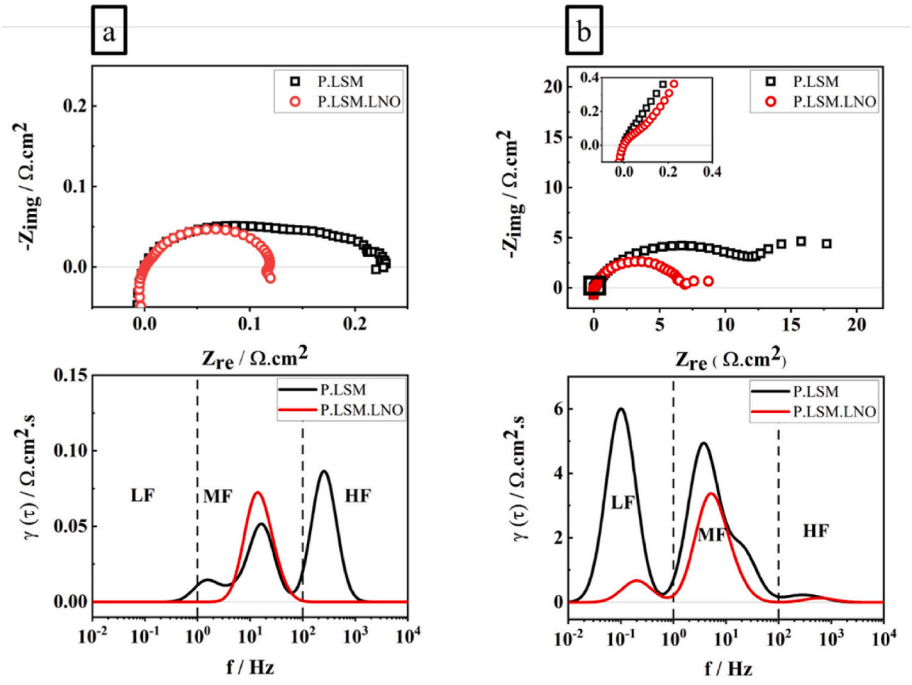

Fig. 6. EIS and DRT analysis for P.LSM and P.LSM.LNO electrodes under (a) +0.3 V DC bias, and (b) −0.3 V DC bias after 10 h of anodic and cathodic polarizations, respectively.

P.LSM.LNO in which the former reached 21.03 Ω cm^2 while the latter increased to 7.62 Ω cm^2. This difference suggests that the LNO nanoparticles promoted the ORR activity of LSM even after the possible intense alterations resulting in the diminution of the nanoparticles surface exchange kinetics. According to the DRT plot in P.LSM.LNO electrode, the rate determining step is the oxygen dissociative adsorption, showing that unlike the P.LSM sample, the oxygen supply to the active sites (gas diffusion) is not the limiting subprocess. Therefore, although it is plausible that the LNO's surface lost its activity through the cathodic polarization, the TPB extension after LNO impregnation have culminated in a less intensive OPP leading to the occurrence of oxygen dissociative adsorption throughout the electrode's thickness [12,16,39]. In addition, it is noteworthy that the absence of the semi-linear part at the HF section of the P.LSM.LNO's EIS spectra could be due to the lower amount of Cr-containing phases on the electrolyte surface at the vicinity of the electrode/electrolyte. Thus, it could be possible to conclude that the reaction products of the LNO/Cr interaction did not totally deteriorate the electrochemical activity of the electrodes, since the infiltrated samples are showing some tolerance towards the presence of Cr content specifically under the anodic polarization.

To exclude the effect of current passage on the R_P evolution and investigate the sole effect of LNO's intrinsic changes and potent reactions between LNO and Cr species, EIS measurements were carried out on the LSM.LNO electrode aged at OCP and 800 °C in the presence and absence of Cr (Fig. 7). In Cr-free atmosphere, R_P of LSM.LNO continuously increases from 0.68 to 1.6 Ω cm^2 which is like the behavior depicted in Fig. 3-b for the LSM.LNO samples during either cathodic or anodic polarization. Thus, the presence of LNO nanoparticles in the SOC's operating condition would be accompanied by R_P increment regardless of being at OCP or under polarization [41,42,44]. This behavior could have been due to the LNO's susceptivity to surface reconstruction specifically when it was present in nanostructured crystals in which the cations segregation would be more likely to happen, due to shorter cation diffusion paths [43,70]. Interestingly, according to Fig. 7, the addition of Cr into the system culminated in R_P reduction to 1.52 Ω cm^2 following its' initial rise from 1.2 to 1.97 Ω cm^2. This R_P reduction could have happened due to the reaction between the formed nucleation agents on the LNO's surface and Cr leading to the formation of a less destructive compounds, e.g., $LaCrO_3$. The R_P reduction in the infiltrated samples at OCP and under cathodic polarization (Fig. 3-a), could be interpreted by the idea that the formation of $LaCrO_3$ have partially reduced the negative effects of La segregation [37,38,45]. While the OCP aged LSM.LNO sample's final R_P is still higher than the initial value (1.52 compared to 1.2 Ω cm^2), in P.LSM.LNO cathode (Fig. 3-a), the electrode became activated, and its' R_P reduced with respect to its' pre-polarization stage. Hence, the activation-like behaviour under cathodic current may be lied in the formation of $LaCrO_3$ since this material is a predominant electron conductor like LSM. Therefore, under cathodic condition, two parameters may have participated in the electrode's LSM-like polarization behavior including LNO's inability to transfer O^{2-} ions through its lattice, and the formation of less active $LaCrO_3$ on the LNO's surface as its' only active path under this condition [61,63]. These parameters may have transferred the electrode's active path towards the interfacial region and make the system ready for LSM's activation [42,45,63].

P.LSM.LNO anode differently behaved compared to the OCP treated LSM.LNO electrode in the presence of Cr. Observation of the P.LSM.LNO anode's R_P and polarization trend (Fig. 2-a, and 3-a) suggests that under the anodic condition formation of La_2O_3 could have been plausible as it was also mentioned by Tong et al. [41]. However, the negative consequences of the LNO's surface reconstruction on the electrode's performance is inhibited by further polarization after 120 min. It would be possible that the secondary phase formation compensates the negative effect of initial insulator phase formation. Nonetheless, the reaction kinetics between LNO and Cr might not be as high as it is in the cathodic or OCP conditions leading to the stabilization trend instead of a reducing one. Egger et al. [45] specified that in the SOEC mode, the higher tolerance of LNO to Cr might be due to the reverse direction of the evolved O_2 gas toward Cr in gas phase. In addition to the opposite oxygen gas flow, it was previously stated that under anodic condition the LNO material exhibits two active paths for oxygen transportation including its' bulk diffusion routes which would not be deteriorated as a result of surface reaction [63]. Considering the abovementioned results, the Cr containing phase which would have been formed on the surface of LNO nanoparticles could have promoted the electrocatalytic activity of the electrodes in comparison with the initial stages in which La cations might have segregated.

Furthermore, Fig. 7 -b and -c in addition to Table 3 represents the FESEM images and EDS analysis correspond to the OCP aged samples (Fig. 7-a). Fig. 7-b shows that the LNO nanoparticles were uniformly distributed within the electrode's bulk and their approximate mean particle size is 70 nm. On the other hand, presence of Cr at high temperatures (800 °C) facilitated the LNO nanoparticle coarsening to the average size of 110 nm (Fig. 7-c). According to the EDS results of the points 1 and 2 taken from LNO nanoparticles in Table 3, 1.08 wt% (0.82

Table 3
EDS analysis of the points noted in Fig. 7.

Elements	Point 1 (wt%)	Point 2 (wt%)
O	27.28	27.11
Cr	1.08	1.57
Mn	19.21	19.26
Ni	1.96	2.79
Sr	16.34	15.45
La	34.13	33.82
Total	100	100

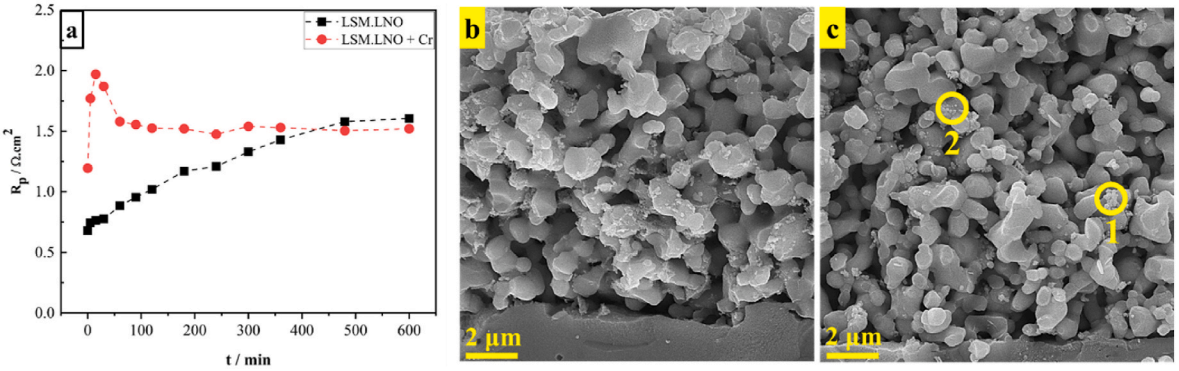

Fig. 7. Polarization resistance trend of (a) the OCP aged LSM.LNO electrode at 800 °C in the absence and presence of Cr, in addition to these samples' FESEM micrographs after 10 h of being (c) in the absence, and (c) in the presence of Cr (Circles represent the points which EDS analysis obtained from).

at.%) and 1.57 wt% (1.19 at.%) Cr are detected, showing that the Cr/LNO reaction was also occurred at OCP. However, the amount of Cr was lower than the one identified in P.LSM.LNO samples polarized anodically and cathodcially.

To clarify what would be produced after LNO and Cr reaction, a reactivity study by means of XRD was conducted. For this purpose, LNO powder was mixed with 5 and 30 wt% of Cr_2O_3 and heated for 12 h at 800 °C for the XRD analysis. According to Fig. 8, the diffraction patterns confirms the formation of $LaCrO_3$ perovskite which was assumed earlier in this study and mentioned in previous investigations [37,38]. In LNO +5 wt% Cr_2O_3 mixture, the Cr_2O_3 peaks are totally and the LNO peaks are partially disappeared. Also, LNO's main diffraction peak shifted towards the lower angles indicating the partial formation of $LaCrO_3$ phase that has a main diffraction peak at lower angles. Raising the Cr_2O_3 to 30 wt%, ends up in formation of $LaCrO_3$ and NiO products in addition to some unreacted Cr_2O_3 after relative disappearance of LNO peaks. Hence, due to the sluggish reaction at the testing cells scale because of the solid/gas interaction, it is reasonable to assume that on the LNO nanoparticles' surface as the most favoured reaction sites, $LaCrO_3$ product would have been formed.

As the newly formed $LaCrO_3$ product continues to form on the LNO surface under continuous cathodic polarization, higher degradation was observed in $\eta_{cathodic}$ for the P.LSM.LNO electrode. Typically, the electrochemical performance of bare LSM electrode strongly depends on the interfacial region for ORR which would cause this electrode's electrochemical performance decay when exposed to a Cr containing atmosphere (Fig. 6-b, 2-a, and 3-a). Because of $LaCrO_3$'s similar characteristics with LSM and its' gradual formation on P.LSM.LNO, the electrode's active area for ORR would have become more confined on the interfacial region leading to a continuous $\eta_{cathodic}$ increment. Consequently, Mn^{2+} ions and oxygen vacancies would have been evolved on the surface of the electrode near the electrolyte, leading to the electrode's activation-like behavior and formation of Cr-containing phases nearby the electrode/electrolyte interface. The anodic polarization of P.LSM.LNO also comprised the initial performance decay due to the possible LNO's surface reconstruction, but further polarization led to R_P and η_{anodic} stabilization. $LaCrO_3$ formation could have been the reason behind the stabilization instead of improvement. The reversed flow of the evolved O_2 could have reduced $LaCrO_3$ formation rate resulting in a competition between this phase production and La-segregation. Moreover, the higher activity of LNO's bulk during anodic condition could have assisted the stability of the electrode's performance towards OER.

Furthermore, as shown by FESEM images in Fig. 5, LNO nanoparticles and $LaCrO_3$ on their surface retarded the formation of Cr and Mn containing phases at the electrode/electrolyte interface after cathodic polarization. However, in prolonged polarization intervals the LNO existence might have not inhibited Cr_2O_3 and $(Cr,Mn)_3O_4$ generation. In the anodically polarized P.LSM.LNO, the presence of LNO nanoparticles substantially supressed the formation of Sr-Cr containing nanoparticles near the electrode/electrolyte interface demonstrating the positive effect of LNO impregnation on the anodic polarization of LSM at the presence of Cr.

LNO nanoparticles impregnation resulted in enhancement of the LSM electrode's electrochemical performance as well as its' tolerance against the presence of Cr in the ambient. For instance, in P.LSM.LNO anode, regardless of its' initial deactivation, the η_{anodic} and R_P values were not only lower, but also more stable than the values attributed to P.LSM anode. Nevertheless, the performance of the P.LSM.LNO cathode indicates that utilization of LNO nanoparticles under cathodic polarization requires to be implemented in a more cautious manner. Although the P.LSM.LNO cathode showed lower $\eta_{cathodic}$ and R_P rather than the P.LSM during the initial stages of the cathodic polarization, it continuously lost its' electrochemical activity and showed similar features to the non-infiltrated P.LSM cathode. It is evident from Figs. 5 and 8 that the LNO nanoparticles were properly distributed, but LNO did not fully cover the LSM's exposed surfaces. In the previous work on the Cr poisoning of the PBSCF cathode, LNO introduction extremely promoted PBSCF's Cr tolerance showing the effects of an optimized coating procedure [32]. Moreover, utilization of La-deficient LNO material was demonstrated to be effective on its' stability within the oxygen containing atmospheres since it suppresses La segregation on its' surface [35]. Therefore, it could be suggested to investigate the effect of La-deficient LNO infiltration into the LSM electrode under SOFC mode to evaluate its' electrochemical properties and Cr poisoning.

4. Conclusion

Stability and performance of the LNO-infiltrated LSM (LSM.LNO) material as the air electrode of SOCs is evaluated in the presence and absence of Cr. Electrochemical and structural characteristics of LSM.LNO electrode were investigated under three distinctive conditions of cathodic, anodic and OCP. Under anodic polarization P.LSM.LNO's R_P and η_{anodic} values increased by about 2.6- and 1.6- fold after 120 min possibly due to LNO's structural variation, however, R_P and η_{anodic} tendencies did not show any sign of further performance deterioration. By the polarization test termination, these values were still lower than the P.LSM anode demonstrating the higher performance of the infiltrated

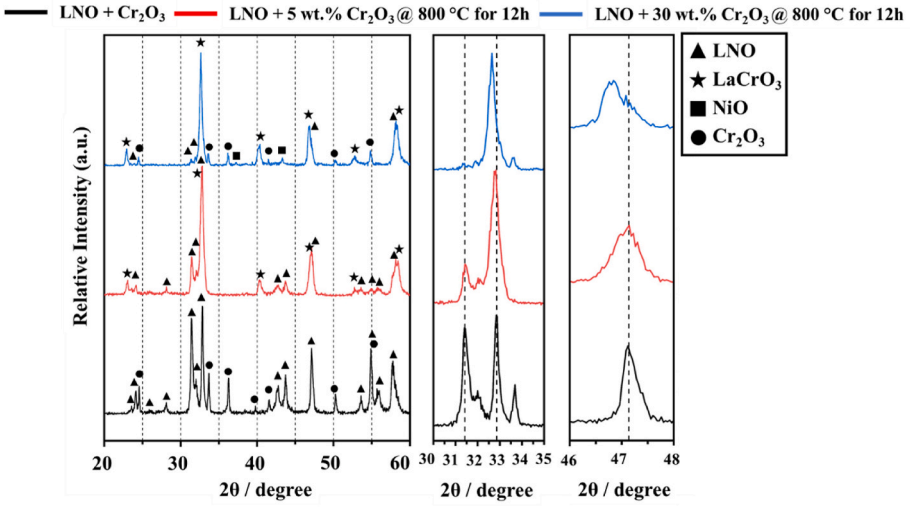

Fig. 8. X-ray diffraction pattern of LNO and Cr_2O_3 mixture before and after heat treatment at 800 °C for 12 h.

electrode under anodic polarization. The microstructural evaluation also revealed that the presence of LNO, regardless of its' structural variations and its' possible reaction with Cr, prevented the Sr-segregation and the possible formation of Sr-Cr containing phases at the area adjacent to anode/electrolyte interface. Under cathodic polarization, P.LSM.LNO's $\eta_{cathodic}$ gradually increased from 157 to 1100 mV within the 600 min of current passage, while in P.LSM cathode this value instantly reached 1400 from 373 mV only after 60 min. On the other hand, P.LSM.LNO cathode's R_P initially increased from 1.05 to 1.70 Ω cm^2 after 30 min, but then began to reduce reaching 0.55 Ω cm^2 after 600 min. During the initial stages, LNO's presence led to suppression of the LSM backbone's dependency on the electrode/electrolyte interface for ORR in addition to a light OPP gradient during the polarization. However, in P.LSM.LNO, the simultaneous structural variation of LNO and interaction with Cr content culminated in the cathode's increased reliance on its' interfacial region and OPP gradient intensification within the electrode's thickness. Therefore, based on the electrochemical data, while the P.LSM.LNO cathode became activated and oxygen vacancies started to form, surface exchange reaction was impeded and $\eta_{cathodic}$ gradually increased. Additionally, in cathodic condition, LNO's presence only postponed, but not inhibited the reaction between the formed nucleation agents (e.g., Mn ions) and Cr on the electrolyte surface. At OCP, the possible LNO's surface reconstruction culminated in continuous R_P increment in the LSM.LNO sample in Cr-free condition, while in the presence of Cr, R_P increment occurred only during the initial 30 min and afterwards it began to reduce. This R_P transition indicates that the possible phases formed on the surface of the LNO nanoparticles led to the electrochemical activity improvement since they might have possessed some electrocatalytic activity. Furthermore, the chemical reactivity study of the LNO and Cr_2O_3 confirmed the formation of $LaCrO_3$ as the major product. The predominant electron conduction nature of $LaCrO_3$ resulted in prevention of the electrode's activity degradation. The stabilized OER performance of the P.LSM.LNO anode could have been brought up by the higher activity of LNO's bulk under the anodic polarization as well as the $LaCrO_3$ lower formation rate under this condition. However, under the cathodic polarization P.LSM.LNO's performance degraded, due to the facts that the formed $LaCrO_3$ is in nature similar to LSM and LNO's activity was confined to the surface diffusion instead of both surface and bulk diffusion. Thus, utilization of LSM.LNO as a cathode material requires to be restricted unless the LNO's stability increase. Nonetheless, LNO-impregnated LSM as the anode of SOEC is a much more reliable choice to be further investigated or even exploited.

CRediT authorship contribution statement

Hirad Salari: Investigation, Writing – original draft, Formal analysis. **Arsalan Zare:** Investigation, Writing – original draft, Formal analysis. **Alireza Babaei:** Conceptualization, Methodology, Resources, Writing – review & editing, Project administration, Supervision. **Hamid Abdoli:** Conceptualization, Methodology, Resources, Writing – review & editing, Project administration, Supervision. **Hamed Aslannejad:** Conceptualization, Writing – review & editing.

Declaration of competing interest

The authors declare that they have no known competing financial interests or personal relationships that could have appeared to influence the work reported in this paper.

Data availability

Data will be made available on request.

Appendix A. Supplementary data

Supplementary data to this article can be found online at https://doi.org/10.1016/j.jpowsour.2023.234001.

References

[1] C. Harrison, P. Slater, R. Steinberger-Wilckens, A review of Solid Oxide Fuel Cell cathode materials with respect to their resistance to the effects of chromium poisoning, Solid State Ionics 354 (2020) 115410.

[2] A. Aphale, et al., Cathode degradation from airborne contaminants in solid oxide fuel cells: a Review, Solid Oxide Fuel Cell Lifetime and Reliability (2017) 101–119.

[3] S.P. Jiang, X. Chen, Chromium deposition and poisoning of cathodes of solid oxide fuel cells – a review, Int. J. Hydrogen Energy 39 (1) (2014) 505–531.

[4] K. Chen, Materials degradation of solid oxide electrolysis cells, J. Electrochem. Soc. 163 (11) (2016) F3070.

[5] P. Lesani, et al., Nanostructured $MnCo_2O_4$ synthesized via co-precipitation method for SOFC interconnect application, Int. J. Hydrogen Energy 41 (45) (2016) 20640–20649.

[6] H. Abdoli, S. Molin, H. Farnoush, Effect of interconnect coating procedure on solid oxide fuel cell performance, Mater. Lett. 259 (2020) 126898.

[7] X. Chen, et al., Interaction between (La, Sr)MnO_3 cathode and Ni–Mo–Cr metallic interconnect with suppressed chromium vaporization for solid oxide fuel cells, Int. J. Hydrogen Energy 34 (14) (2009) 5737–5748.

[8] K. Chen, S.P. Jiang, Degradation and durability of electrodes of solid oxide fuel cells, Materials for High-Temperature Fuel Cells (2013) 245–307.

[9] J.T. Irvine, P. Connor, Solid oxide fuels cells: facts and figures, Springer 233 (2013).

[10] K. Chen, et al., Chromium deposition and poisoning of $La_{0.8}Sr_{0.2}MnO_3$ oxygen electrodes of solid oxide electrolysis cells, Faraday Discuss 182 (2015) 457–476.

[11] Y. Zhen, Transition behavior for O_2 reduction reaction on (La, Sr)MnO_3/ YSZ composite cathodes of solid oxide fuel cells, J. Electrochem. Soc. 153 (12) (2006) A2245.

[12] Y. Zhen, J. Li, Oxygen reduction on strontium-doped $LaMnO_3$ cathodes in the absence and presence of an iron–chromium alloy interconnect, J. Power Sources 162 (2) (2006) 1043–1052.

[13] S. He, et al., A critical review of key materials and issues in solid oxide cells, Interdisciplinary Materials 2 (1) (2023) 111–136.

[14] X. Chen, L. Zhang, E. Liu, A fundamental study of chromium deposition and poisoning at $(La_{0.8}Sr_{0.2})_{0.95}(Mn_{1-x}Co_x)O_{3\pm\delta}$ $(0.0 \leq x \leq 1.0)$ cathodes of solid oxide fuel cells, Int. J. Hydrogen Energy 36 (1) (2011) 805–821.

[15] S. Jiang, J. Zhang, K. Foger, Deposition of chromium species at Sr-doped $LaMnO_3$ electrodes in solid oxide fuel cells: III. Effect of air flow, J. Electrochem. Soc. 148 (7) (2001) C447.

[16] S. Jiang, J. Zhang, K. Foger, Deposition of chromium species at Sr-doped $LaMnO_3$ electrodes in solid oxide fuel cells II, Effect on O_2 Reduction Reaction. Journal of the Electrochemical Society 147 (9) (2000) 3195.

[17] S. Jiang, et al., Deposition of chromium species at Sr-Doped $LaMnO_3$ electrodes in solid oxide fuel cells, I. mechanism and kinetics. Journal of the Electrochemical Society 147 (11) (2000) 4013.

[18] X. Chen, K. Khor, S. Chan, Electrochemical behavior of La(Sr)MnO_3 electrode under cathodic and anodic polarization, Solid State Ionics 167 (3–4) (2004) 379–387.

[19] X. Chen, S. Chan, K. Khor, Defect chemistry of $La_{1-x}Sr_xMnO_{3\pm\delta}$ under cathodic polarization, Electrochem. Solid State Lett. 7 (6) (2004) A144.

[20] Y. Zhang, et al., A model for the delamination kinetics of $La_{0.8}Sr_{0.2}MnO_3$ oxygen electrodes of solid oxide electrolysis cells, Int. J. Hydrogen Energy 37 (19) (2012) 13914–13920.

[21] K. Chen, Failure mechanism of (La, Sr)MnO_3 oxygen electrodes of solid oxide electrolysis cells, Int. J. Hydrogen Energy 36 (17) (2011) 10541–10549.

[22] A. Babaei, L. Zhang, E. Liu, Performance and stability of $La_{0.8}Sr_{0.2}MnO_3$ cathode promoted with palladium based catalysts in solid oxide fuel cells, J. Alloys Compd. 509 (14) (2011) 4781–4787.

[23] W. Wang, Fabrication and performance of GDC-impregnated (La,Sr)MnO_3 cathodes for intermediate temperature solid oxide fuel cells, J. Electrochem. Soc. 152 (7) (2005) A1398.

[24] K. Chen, N. Ai, Development of $(Gd,Ce)O_2$-impregnated (La,Sr)MnO_3 anodes of high temperature solid oxide electrolysis cells. Journal of the Electrochemical Society 157 (11) (2010) P89.

[25] Z. Jiang, et al., Bismuth oxide-coated (La,Sr)MnO_3 cathodes for intermediate temperature solid oxide fuel cells with yttria-stabilized zirconia electrolytes, Electrochim. Acta 54 (11) (2009) 3059–3065.

[26] N. Ai, et al., Nanostructured $(Ba,Sr)(Co,Fe)O_{3-\delta}$ impregnated (La,Sr)MnO_3 cathode for intermediate-temperature solid oxide fuel cells. Journal of the Electrochemical Society 157 (7) (2010) B1033.

[27] S. Seyed-Vakili, et al., Performance improvement of an inhomogeneous cathode by infiltration, Fuel Cell. 17 (1) (2017) 108–114.

[28] S. Shahrokhi, A. Babaei, C. Zamani, Reversible operation of $La_{0.8}Sr_{0.2}MnO_3$ oxygen electrode infiltrated with Ruddlesden-Popper and perovskite lanthanum nickel cobaltite, Int. J. Hydrogen Energy 43 (52) (2018) 23091–23100.

[29] Z. Akbari, A. Babaei, Electrochemical performance of $La_{0.8}Sr_{0.2}MnO_3$ oxygen electrode promoted by Ruddlesden-Popper structured La_2NiO_4, J. Am. Ceram. Soc. 103 (2) (2020) 1332–1342.

[30] S.P. Jiang, Nanoscale and nano-structured electrodes of solid oxide fuel cells by infiltration: advances and challenges, Int. J. Hydrogen Energy 37 (1) (2012) 449–470.

[31] J. Huang, et al., A hybrid catalyst coating for a high-performance and chromium-resistive cathode of solid oxide fuel cells, Chem. Eng. J. 431 (2022) 134281.

[32] J. Li, et al., Promoted Cr-poisoning tolerance of $La_2NiO_{4+\delta}$-coated $PrBa_{0.5}Sr_{0.5}Co_{1.5}Fe_{0.5}O_{5+\delta}$ cathode for intermediate temperature solid oxide fuel cells, Electrochim. Acta 270 (2018) 294–301.

[33] X. Zhang, H. Zhang, X. Liu, High performance $La_2NiO_{4+\delta}$-infiltrated $(La_{0.6}Sr_{0.4})_{0.995}Co_{0.2}Fe_{0.8}O_{3-\delta}$ cathode for solid oxide fuel cells, J. Power Sources 269 (2014) 412–417.

[34] S. Choi, et al., High performance sofc cathode prepared by infiltration of $La_{n+1}Ni_nO_{3n+1}$ (n= 1, 2, and 3) in porous ysz, J. Electrochem. Soc. 158 (8) (2011) B995.

[35] X. Zhang, et al., A-site deficient $La_{2-X}NiO_{4+\delta}$ infiltrated LSCF cathode with improved performance and stability, ECS Trans. 78 (1) (2017) 593.

[36] M. Ghamarinia, A. Babaei, C. Zamani, Electrochemical characterization of $La_2NiO_{4+\delta}$ infiltrated $La_{0.6}Sr_{0.4}Co_{0.2}Fe_{0.8}O_{3-\delta}$ by analysis of distribution of relaxation times, Electrochim. Acta 353 (2020) 136520.

[37] S.-N. Lee, A. Atkinson, J.A. Kilner, Chromium poisoning of $La_2NiO_{4+\delta}$ cathodes, ECS Trans. 57 (1) (2013) 605.

[38] N. Schrödl, et al., Phase decomposition of $La_2NiO_{4+\delta}$ under Cr-and Si-poisoning conditions, Solid State Ionics 322 (2018) 44–53.

[39] A.A. Solodyankin, et al., Revealing the degradation mechanism of the lanthanum nickelates based double-layer electrodes during long-term tests in contact with chromium-containing steel interconnects, Int. J. Energy Res. 46 (9) (2022) 12579–12596.

[40] K. Hilpert, et al., Chromium vapor species over solid oxide fuel cell interconnect materials and their potential for degradation processes, J. Electrochem. Soc. 143 (11) (1996) 3642.

[41] X. Tong, et al., Performance and stability of Ruddlesden-Popper $La_2NiO_{4+\delta}$ oxygen electrodes under solid oxide electrolysis cell operation conditions, Ceram. Int. 43 (14) (2017) 10927–10933.

[42] Z. He, et al., Positive effect of incorporating $Er_{0.4}Bi_{1.6}O_3$ on the performance and stability of $La_2NiO_{4+\delta}$ cathode, J. Electrochem. Soc. 166 (12) (2019) F796.

[43] J. Wu, et al., Why Ni is absent from the surface of $La_2NiO_{4+\delta}$, J. Mater. Chem. A 3 (47) (2015) 23760–23767.

[44] K.-T. Wu, et al., Surface chemistry and restructuring in thin-film $La_{n+1}Ni_nO_{3n+1}$ (n= 1, 2 and 3) Ruddlesden–Popper oxides, J. Mater. Chem. A 5 (19) (2017) 9003–9013.

[45] A. Egger, et al., $La_2NiO_{4+\delta}$ as electrode material for solid oxide fuel cells and electrolyzer cells, Solid State Ionics 299 (2017) 18–25.

[46] A. Zare, et al., Electrochemical evaluation of $Sr_2Fe_{1.5}Mo_{0.5}O_{6-\delta}/Ce_{0.9}Gd_{0.1}O_{1.95}$ cathode of SOFCs by EIS and DRT analysis, J. Electroanal. Chem. 936 (2023) 117376.

[47] D.A. Osinkin, An approach to the analysis of the impedance spectra of solid oxide fuel cell using the DRT technique, Electrochim. Acta 372 (2021) 137858.

[48] B. Zhang, et al., Nanofiber $Sr_2Fe_{1.5}Mo_{0.5}O_{6-\delta}$ electrodes fabricated by the electrospinning method for solid-oxide cells, Crystals 12 (11) (2022) 1624.

[49] A. Montenegro-Hernández, et al., Thermal stability of $Ln_2NiO_{4+\delta}$ (Ln: La, Pr, Nd) and their chemical compatibility with YSZ and CGO solid electrolytes, Int. J. Hydrogen Energy 36 (24) (2011) 15704–15714.

[50] R. Sayers, S. Skinner, Evidence for the catalytic oxidation of $La_2NiO_{4+\delta}$, J. Mater. Chem. 21 (2) (2011) 414–419.

[51] S. Zhang, Y. Zhen, Deposition of Cr species at $(La,Sr)(Co,Fe)O_3$ cathodes of solid oxide fuel cells, J. Electrochem. Soc. 153 (1) (2005) A127.

[52] X. Chen, et al., Study on the Cr deposition and poisoning phenomenon at $(La_{0.6}Sr_{0.4})(Co_{0.2}Fe_{0.8})O_{3-\delta}$ electrode of solid oxide fuel cells by transmission X-ray microscopy, Int. J. Hydrogen Energy 39 (28) (2014) 15728–15734.

[53] M. Ghamarinia, et al., Application of the distribution of relaxation time method in electrochemical analysis of the air electrodes in the SOFC/SOEC devices: a review, Chemical Engineering Journal Advances (2023) 100503.

[54] T. Yang, et al., $(La_{0.8}Sr_{0.2})_{0.98}MnO_{3-\delta}$-$Zr_{0.92}Y_{0.16}O_{2-\delta}$: PrO_x for oxygen electrode supported solid oxide cells, Appl. Catal. B Environ. 306 (2022) 121114.

[55] M. Wei, et al., High performance $La_2NiO_{4+\delta}$ impregnated $La_{0.6}Sr_{0.4}Co_{0.2}Fe_{0.8}O_{3-\delta}$ cathodes for solid oxide fuel cells, Solid State Ionics 387 (2022) 116065.

[56] Y. Gao, et al., Cr deposition and poisoning on $SrCo_{0.9}Ta_{0.1}O_{3-\delta}$ cathode of solid oxide fuel cells, Int. J. Hydrogen Energy 48 (6) (2023) 2341–2350.

[57] Y. Gao, et al., Cr deposition and poisoning on $SrCo_{0.9}Ta_{0.1}O_{3-\delta}$ cathode of solid oxide fuel cells, Int. J. Hydrogen Energy 48 (6) (2023) 2341–2350.

[58] M. Sugimoto, Chromium Poisoning Mitigation in Solid Oxide Fuel Cell Air Electrodes: Mechanisms for Cr Deposition and Removal, Boston University, 2022.

[59] J. Druce, et al., Surface termination and subsurface restructuring of perovskite-based solid oxide electrode materials, Energy Environ. Sci. 7 (11) (2014) 3593–3599.

[60] V.I. Sharma, B. Yildiz, Degradation mechanism in $La_{0.8}Sr_{0.2}CoO_3$ as contact layer on the solid oxide electrolysis cell anode, J. Electrochem. Soc. 157 (3) (2010) B441.

[61] P. Qiu, et al., $LaCrO_3$-Coated $La_{0.6}Sr_{0.4}Co_{0.2}Fe_{0.8}O_{3-\delta}$ core–shell structured cathode with enhanced Cr tolerance for intermediate-temperature solid oxide fuel cells, ACS Appl. Mater. Interfaces 12 (26) (2020) 29133–29142.

[62] C. Peng, B. Wang, A. Vincent, $LaCrO_3$–VO_x–YSZ anode material for solid oxide fuel cells operating on H_2S-containing syngas, J. Mater. Sci. 47 (2012) 227–233.

[63] G. Sdanghi, et al., Reaction mechanisms of $La_2NiO_{4+\delta}$ oxygen electrodes operated in electrolysis and fuel cell mode, J. Electrochem. Soc. 169 (3) (2022) 34518.

[64] K. Chen, S.P. Jiang, Surface segregation in solid oxide cell oxygen electrodes: phenomena, mitigation strategies and electrochemical properties, Electrochem. Energy Rev. 3 (2020) 730–765.

[65] J. Li, et al., The investigation of Cr deposition and poisoning effect on Sr-doped lanthanum manganite cathode induced by cathodic polarization for intermediate temperature solid oxide fuel cell, Electrochim. Acta 255 (2017) 31–40.

[66] J. Zamudio-García, et al., Boosting the performance of $La_{0.8}Sr_{0.2}MnO_{3-\delta}$ electrodes by the incorporation of nanocomposite active layers, Adv. Mater. Interfac. 9 (22) (2022) 2200702.

[67] J. Wang, et al., Ta-Doped $SrCoO_{3-\delta}$ as a promising bifunctional oxygen electrode for reversible solid oxide fuel cells: a focused study on stability. Journal of Materials Chemistry A 5 (19) (2017) 8989–9002.

[68] H.A. Ishfaq, et al., A heuristic approach to boost the performance and Cr poisoning tolerance of solid oxide fuel cell cathode by robust multi-doped ceria coating, Appl. Catal. B Environ. 323 (2023) 122178.

[69] S. Taniguchi, et al., Degradation phenomena in the cathode of a solid oxide fuel cell with an alloy separator, J. Power Sources 55 (1) (1995) 73–79.

[70] K. Develos-Bagarinao, et al., Oxygen surface exchange properties and surface segregation behavior of nanostructured $La_{0.6}Sr_{0.4}Co_{0.2}Fe_{0.8}O_{3-\delta}$ thin film cathodes, Phys. Chem. Chem. Phys. 21 (13) (2019) 7183–7195.